

This work was written as part of one of the author's official duties as an Employee of the United States Government and is therefore a work of the United States Government. In accordance with 17 U.S.C. 105, no copyright protection is available for such works under U.S. Law.

Public Domain Mark 1.0

<https://creativecommons.org/publicdomain/mark/1.0/>

Access to this work was provided by the University of Maryland, Baltimore County (UMBC) ScholarWorks@UMBC digital repository on the Maryland Shared Open Access (MD-SOAR) platform.

**Please provide feedback**

Please support the ScholarWorks@UMBC repository by emailing [scholarworks-group@umbc.edu](mailto:scholarworks-group@umbc.edu) and telling us what having access to this work means to you and why it's important to you. Thank you.



# Titan's plasma environment: 3D hybrid kinetic modeling of the TA flyby and comparison with CAPS-ELS and RPWS LP observations

A.S. Lipatov<sup>a,b,\*</sup>, E.C. Sittler Jr.<sup>c</sup>, R.E. Hartle<sup>c</sup>, J.F. Cooper<sup>c</sup>, D.G. Simpson<sup>c</sup>

<sup>a</sup> GPHI UMBC/NASA GSFC, Code 673, Greenbelt, MD 20771, USA

<sup>b</sup> Faculty of Problems of Physics and Power Engineering, Moscow Institute of Physics and Technology, Russia

<sup>c</sup> NASA Goddard Space Flight Center, Greenbelt, MD 20771, USA

## ARTICLE INFO

### Article history:

Received 27 June 2013

Received in revised form

14 February 2014

Accepted 21 February 2014

Available online 5 March 2014

### Keywords:

Ionospheres

Atmospheres

Induced magnetospheres

Magnetic barrier

Alfvén wing

Satellites

Pickup ion

## ABSTRACT

In this report we discuss the global plasma environment of the TA flyby from the perspective of 3D hybrid modeling. In our model the background, pickup, and ionospheric ions are considered as particles, whereas the electrons are described as a fluid. Inhomogeneous photoionization, electron-impact ionization and charge exchange are included in our model. We also take into account the collisions between the ions and neutrals. Our modeling shows that mass loading of the background plasma ( $H^+$ ,  $O^+$ ) by pickup ions  $H_2^+$ ,  $CH_4^+$  and  $N_2^+$  differs from the T9 encounter simulations when  $O^+$  ions are not introduced into the background plasma. In our hybrid modeling we use Chamberlain profiles for the atmospheric components. We also include a simple ionosphere model with average mass  $M=28$  amu ions that were generated inside the ionosphere. Titan's interior is considered as a weakly conducting body. Special attention has been paid to comparing the simulated pickup ion density distribution with CAPS-ELS and with RPWS LP observations by the Cassini–Huygens spacecraft along the TA trajectory. Our modeling shows an asymmetry of the ion density distribution and the magnetic field, including the formation of Alfvén wing-like structures.

© 2014 Elsevier Ltd. All rights reserved.

## 1. Introduction

On July 1, 2004, the Cassini spacecraft began observational studies of the Saturnian system. The TA encounter on October 26, 2004 was the first low-altitude pass through Titan's upper atmosphere by the Cassini–Huygens spacecraft. The TA flyby provided important information concerning the ion and neutral composition and plasma dynamics below the exobase and inside the exosphere. The Cassini Plasma Spectrometer (CAPS) has three independently operated sensors (Young et al., 2004): the ion mass spectrometer (IMS), designed to analyze ion composition and plasma dynamics; the electron spectrometer (ELS); and the ion beam spectrometer (IBS) to measure narrow, beam-like distributions without mass separations. CAPS data together with the Langmuir Probe (LP) and Cassini magnetometer (MAG) data (Dougherty et al., 2004) and appropriate computational models present a strong tool for a study the dynamic processes in Titan's environment. Wave–particle interactions play a very important role in plasma dynamics near Titan: mass loading, excitation of low-frequency waves and the formation of the particle velocity

distribution function (e.g., ring/shell-like distributions, etc.). The kinetic approach is important for the estimation of collision processes (e.g., a charge exchange). Particle–wave interactions play a very important role in the possible formation of a shock wave or an Alfvén wing, and in coupling of pickup ions and background ions via excitation of low-frequency waves. These kinetic processes become important in the formation of an obstacle for the background plasma.

Magnetohydrodynamic (MHD) simulations have been useful in the study of the interaction between plasma flow and Titan (Keller and Cravens, 1994; Ledvina and Cravens, 1998; Cravens et al., 1998; Kabin et al., 1999, 2000; Nagy et al., 2001; Ma et al., 2006, 2007; Ledvina et al., 2005; Snowden et al., 2007). MHD simulations demonstrated a global picture of magnetospheric interaction with a moon, including mass loading the magnetosphere's plasma with the atmosphere's pickup ions and possible chemical processes inside the exobase where the fluid approximation is adequate. However, several kinetic effects have been lost, namely an asymmetry in the form of an Alfvén wing and a magnetic barrier near a moon, an asymmetry in the atmosphere's pickup ion distribution, possible plasma structure with a thickness of the order of the heavy ion gyroradius, an overestimate of the pickup ion fluxes along the magnetic field, and the absence of kinetic effects inside plasma structures. Multi-fluid models may produce some kinetic effects like cold ion–beam–beam interactions, but they cannot

\* Corresponding author. Tel.: +1 3012860906; fax: +1 3012861688.

E-mail addresses: [Alexander.Lipatov-1@nasa.gov](mailto:Alexander.Lipatov-1@nasa.gov) (A.S. Lipatov), [Edward.C.Sittler@nasa.gov](mailto:Edward.C.Sittler@nasa.gov) (E.C. Sittler Jr.), [Richard.E.Hartle@nasa.gov](mailto:Richard.E.Hartle@nasa.gov) (R.E. Hartle), [John.F.Cooper@nasa.gov](mailto:John.F.Cooper@nasa.gov) (J.F. Cooper), [David.G.Simpson@nasa.gov](mailto:David.G.Simpson@nasa.gov) (D.G. Simpson).

produce wave–particle interactions due to a thermal ion velocity distribution. Note that the energy due to the thermal velocity of ions is of the same order as the energy due to the bulk velocity inside Titan's exosphere. Many of these effects may be recovered by using hybrid models.

Several 3D hybrid models of Titan plasma interactions were performed during the last decade as described in papers by Brecht et al. (2000), Kallio et al. (2004), Sillanpää et al. (2006), Modolo et al. (2007a,b), Simon et al. (2007), Kallio et al. (2007), Modolo and Chanteur (2008), Ledvina and Brecht (2012), and Ledvina et al. (2012). These simulations were devoted to an interpretation of Voyager 1 (Ness et al., 1982; Hartle et al., 1982) and Cassini data and assumed the presence of the heavy ions like  $O^+$  in magnetospheric plasma. Kallio et al. (2007) discuss hybrid modeling for the T9 case in the presence of  $H_2^+$  and  $H_1^+$  ions in the background plasma. However, they used a higher total density ( $0.4 \text{ cm}^{-3}$ ) for these ions than was observed in the CAPS T9 measurements ( $0.05 \text{ cm}^{-3}$ ) (Sittler et al., 2010). Lipatov et al. (2011, 2012) have provided 3D hybrid modeling of the T9 encounter and have taken into account the absence of  $O^+$  in the background plasma (Sittler et al., 2010). The main results that were obtained in these hybrid models are the following: an asymmetry of a nonstationary bow shock (when Titan's location is outside Saturn's magnetosphere) and the magnetic barrier due to the large gyroradius of magnetospheric ions. Hybrid modeling provided good agreement with observations from the TA and T9 encounters. However, an understanding and interpretation of the CAPS data for the TA encounter requires more complicated models of Titan's atmosphere and ionosphere.

Our study of the neutral atmosphere will be taken from Hartle and Sittler (2006) and Sittler et al. (2005). Photoionization, electron impact and charge exchange rates were taken from Sittler et al. (2005). We apply a time-dependent Boltzmann's "particle in cell" approach (Lipatov et al., 1998), together with a hybrid plasma (ion kinetic) model (Lipatov et al., 2002), in three spatial dimensions (see, e.g., Lipatov and Combi, 2006) using a prescribed but adjustable neutral atmosphere and ionosphere model for Titan. A Boltzmann simulation is applied to model charge exchange between incoming and pickup ions and the immobile atmospheric neutrals. In this paper we discuss the first results of hybrid kinetic modeling of Titan's environment (TA encounter), namely global plasma structures, e.g., the formation of a magnetic barrier, Alfvén wing, pickup ion tail, etc. The results of these kinetic models are compared with Cassini TA flyby observational data (CAPS). A portion of this modeling has been presented in Lipatov et al. (2007a,b,c). Comparison of results of our hybrid model with other Cassini flybys will be presented in a future publication.

The paper is organized as follows. In Section 2 we present the computational model and a formulation of the problem. In Section 3 we present the results of modeling the plasma environment near Titan (TA) and comparison with observational data. Finally, in Section 4 we summarize our results and discuss the future development of our computational model.

## 2. Formulation of the problem and mathematical model

To study the interaction of Saturn's magnetosphere with the ionized and neutral components of Titan's environment we use a quasineutral hybrid model, namely a kinetic description for the background and pickup ions, and a fluid approximation for electrons. The hybrid model accurately describes wave–particle interactions on the following ion spatial ( $\lambda$ ) and time ( $\omega^{-1}$ ) scales:  $\lambda \sim \rho_{ci} = U_0/\Omega_i$  or  $\lambda \sim c/\omega_{pi}$  and  $\lambda \gg \rho_{ce}$ ;  $\omega \leq \Omega_i$ , where  $\rho_{ci}$  and  $\rho_{ce}$  denote the gyroradii for ions and electrons respectively;  $U_0$  is the

bulk velocity of the background plasma;  $c/\omega_{pi}$  denotes the ion inertial length, and  $\Omega_i$  is the ion gyrofrequency. The length  $\lambda$  may represent either the wavelength of the excited low-frequency waves or the spatial scale of the plasma structures and boundaries in the Titan environment. The model includes photoionization, electron impact ionization and charge exchange. We explicitly include ionization, mass-loading and charge exchange as the dominant mechanisms for the interaction away from the lower boundary at Titan. We also include finite conductivity, given by the diffusion scale length, at the inner boundary. The atmosphere is considered to be an immobile component in this paper.

The general scheme of the global interaction of Saturn's magnetosphere with Titan and the Cassini TA trajectory is given in Fig. 1. The Cassini TA flyby occurred nearly in the equatorial plane of Titan and perpendicular to the direction of the plasma wake defined by the corotating plasma flow past Titan. The spacecraft trajectory passed approximately 1174 km ( $1.46 R_T$ ) downstream from Titan (in the sense of the plasma torus flow). In our coordinate system the X-axis is parallel to  $U_0$  (corotational plasma velocity), Y is directed toward Saturn, and Z is directed to the north.

In the hybrid models described here, the dynamics of upstream ions and implanted ions is a kinetic approach, while the dynamics of the electrons is described by a hydrodynamical approximation.

The single particle ion distribution function  $f_s(t, \mathbf{x}, \mathbf{v})$  has to fulfill the Vlasov/Boltzmann equation

$$\frac{\partial f_s}{\partial t} + \mathbf{v} \cdot \frac{\partial f_s}{\partial \mathbf{x}} + \frac{\mathbf{F}}{M_s} \cdot \frac{\partial f_s}{\partial \mathbf{v}} = F_{coll} + P - L_{exch}, \quad (1)$$

where  $\mathbf{F}$  symbolizes forces due to electric and magnetic fields acting on the ions,  $F_{coll}$  is the collision term,  $P$  denotes the production rate of the ions by an ionization and charge exchange, and  $L_{exch}$  the loss rate of ions due to charge exchange at  $(\mathbf{x}, \mathbf{v})$ .  $M_s$  is a mass of an ion of species  $s$ . In this paper we use the particle-mesh model for ion dynamics instead of the Vlasov/Boltzmann equation, Eq. (1).

Single ion particle motion is described by the equations (see, e.g., Eqs. (1) and (14) from Mankofsky et al., 1987)

$$\frac{d\mathbf{r}_{s,l}}{dt} = \mathbf{v}_{s,l} \quad (2)$$

and

$$\frac{d\mathbf{v}_{s,l}}{dt} = \frac{e}{M_s} \left( \mathbf{E} + \frac{\mathbf{v}_{s,l} \times \mathbf{B}}{c} \right) - \frac{m_e U_{ie}}{M_s} (\mathbf{v}_{s,l} - \mathbf{U}_i) - \frac{m_e U_{ie}}{M_s n_i} \mathbf{J} - \nu_{so} \mathbf{v}_{s,l}. \quad (3)$$

Here we assume that the charge state is  $Z_i = 1$ .  $\mathbf{U}_i$  and  $\mathbf{J}$  denote the charge-averaged velocity of all (incoming and pickup) ions and the total current (see Eq. (8)) respectively. Here  $m_e$ ,  $e$ , and  $n_i$  are the

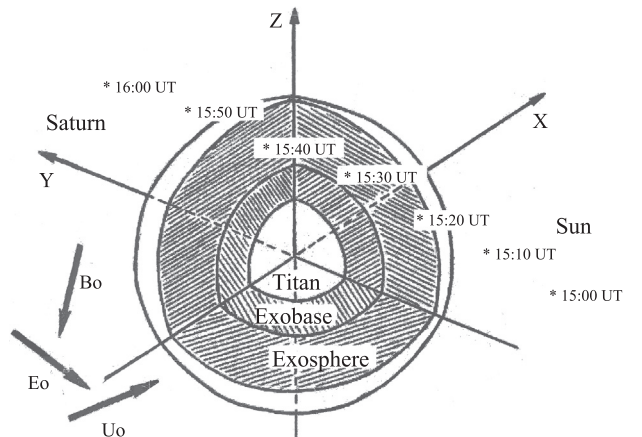


Fig. 1. Titan's plasma environment and the system of coordinates.

electron mass, electron charge, and the total ion density respectively. The subscript  $s$  denotes the ion population ( $s=1,2$  for incoming ions and  $s=3,4,5$  for  $\text{H}_2^+$ ,  $\text{N}_2^+$ ,  $\text{CH}_4^+$  pickup ions;  $s=6$  for ionospheric ions) and the index  $l$  is the particle index.  $\nu_{ie}$  and  $\nu_{io}$  are collision frequencies between ions and electrons, and ions and neutrals that may include Coulomb collisions and collisions due to particle–wave interactions. Note that the collision rates used in Eq. (3) must depend on individual velocities of ions and electrons. However, we use the effective resistivity  $\eta$ ,  $\eta = \sigma^{-1} = m_e / (ne^2 \tau_e)$ , where the characteristic electron collision time  $\tau_e = \nu_{ie}^{-1}$  and  $n$  denotes the total ion density. The electrical conductivities may be estimated as

$$\sigma_{\perp} = \sigma_1 T_e^{3/2}, \quad \sigma_{\parallel} = 1.92 \sigma_{\perp}, \quad \sigma_1 = 0.9 \times 10^{13} / ((\Lambda/10) Z_i) \text{ s}^{-1} \text{ eV}^{-3/2}, \quad (4)$$

where  $T_e$  denotes the electron temperature in eV and  $\Lambda$  is the Coulomb logarithm (see, e.g., Braginskii, 1965, pp. 215–216). For the typical background (upstream) plasma parameters are  $T_e = 200$  eV (electron temperature) and  $n_0 = 0.1 \text{ cm}^{-3}$  (ion density); the electrical conductivities are  $\sigma_{\perp} \approx 4.7 \times 10^{13} \text{ s}^{-1}$  and  $\sigma_{\parallel} \approx 9.2 \times 10^{13} \text{ s}^{-1}$ . Charged particle-neutral collision frequencies are calculated depending on the species in question. For a plasma, the thermal velocity  $v_{\alpha}$  ( $\alpha = i, e$ ) is assumed to be greater than the drift velocity, so we take

$$\nu_{\alpha,0} = n_0 \sigma^{0,\alpha} v_{\alpha}, \quad (5)$$

where the cross section  $\sigma^{0,\alpha}$  is typically about  $5 \times 10^{-15} \text{ cm}^2$  and  $n_0$  is the neutral atmosphere density (see, e.g., Mankofsky et al., 1987, Eq. (17)).

In our modeling we use a low (much smaller than the real value) effective conductivity to suppress “shot” noise and for modeling Titan’s body; hence, we may drop the first collision term on the right-hand side of Eq. (3) for simplicity. We also drop the third collisional term in Eq. (3) for simplicity. We also take into account the interaction of ions with neutral particles by charge exchange (see Lipatov and Combi, 2006, Eqs. (12)–(15)), and we also assume that the bulk velocity and thermal temperatures of neutral particles equal zero.

In the nonradiative limit, Ampère’s law is given by

$$\frac{4\pi}{c} \mathbf{J} = \nabla \times \mathbf{B}; \quad (6)$$

and the induction equation (Faraday’s law) by

$$\frac{1}{c} \frac{\partial \mathbf{B}}{\partial t} + \nabla \times \mathbf{E} = 0. \quad (7)$$

The total current is given by

$$\mathbf{J} = \mathbf{J}_e + \mathbf{J}_i; \quad \mathbf{J}_i = \sum_{s=1}^{N_{\text{species}}} en_s \mathbf{U}_s = en_i \mathbf{U}_i, \quad (8)$$

where  $\mathbf{U}_s$  is the bulk velocity and  $n_s$  is the density of ions of type  $s$ ;  $n_s$  is the total ion density, and  $\mathbf{U}_i$  is the average ion bulk velocity.

We further assume quasi-neutrality

$$n_e = \sum_{s=1}^{N_{\text{species}}} n_s. \quad (9)$$

For massless electrons the equation of motion of the electron fluid takes the form of standard generalized Ohm’s law (e.g., Braginskii, 1965):

$$\mathbf{E} = \frac{\mathbf{J}_e \times \mathbf{B}}{en_e c} - \frac{\nabla p_e}{en_e} - \frac{m_e}{e} \sum_s \nu_{e,s} (\mathbf{U}_i - \mathbf{U}_s) + \frac{m_e}{n_e e^2} \sum_s \nu_{e,s} \mathbf{J} - \frac{m_e \nu_{e,0}}{e} \mathbf{U}_e, \quad (10)$$

where  $p_e = nm_e \langle v_e^2 \rangle / 3 = n_e T_e$  is the scalar electron pressure, and  $v_e'$  is the thermal velocity of electrons; the electron current  $\mathbf{J}_e$  is estimated from Eq. (8). Evaluation of the effective conductivities that correspond to the frequency  $\nu_{e,0}$  gives the following

expression:

$$\sigma_{e,0} = \frac{\omega_{pe}^2}{4\pi \nu_{e,0}} = \frac{\omega_{pe}^2}{4\pi \sigma^{e,0} n_0' v_e'} = \frac{1.64 \times 10^{14} n_e'}{n_0'} s^{-1}, \quad (11)$$

where dimensional values are  $n_e' = n_e / n_0$  (electron density) and  $n_0' = n_0 / n_{\text{atmos}}$  (neutral density, see Eq. (13)). Here  $\omega_{pe}$  is the electron plasma frequency and  $n_0$  is the ion background density. In our modeling we assume that  $|\mathbf{U}_i - \mathbf{U}_s| \ll J / (ne)$  and we drop the third and fifth terms from the right-hand side of Eq. (10).

Since we suppose that electron heating due to collisions with ions is very small, the electron fluid is considered adiabatic. For simplicity we assume that the total electron pressure may be represented as a sum of partial pressures of all electron populations:

$$p_e = p_{e0} \frac{(\beta_e n_{i,\text{up}}^{5/3} + \sum_s \beta_{e,\text{Pl},s} n_{i,\text{Pl},s}^{5/3} + \beta_{e,\text{iono}} n_{i,\text{iono}}^{5/3})}{\beta_e n_0^{5/3}}, \quad (12)$$

where  $\beta_e$ ,  $\beta_{e,\text{Pl},s}$ , and  $\beta_{e,\text{iono}}$  denote electron upwind, pickup and ionosphere betas respectively.  $p_{e0}$  and  $n_0$  are the upstream electron pressure and the ion density respectively. We also assume here that  $n_{e,\text{up}} = n_{i,\text{up}}$ ,  $n_{e,\text{Pl},s} = n_{i,\text{Pl},s}$ , and  $n_{e,\text{iono}} = n_{i,\text{iono}}$ . Here,  $n_{i,\text{iono}}$  denotes the immobile ionosphere ions. Otherwise, we have to calculate the electron pressure from heat balance for electrons (see, e.g., Braginskii, 1965) taking into account the heat fluxes for pickup electrons and ionospheric electrons on the right-hand side of this equation. The ion kinetic approach allows us to take into account the effects of anisotropy of ion pressure, the correct mass loading processes, the penetration of ions across the ionosphere, and the asymmetry of plasma flow around Titan. Remember that the fluid models, which account only for the scalar (i.e., isotropic) ion pressure, may result in an extra-expansion of the pickup ions along the Alfvén wing. Our computational model may also include charge exchange between magnetospheric ions and atmospheric atoms, and between pickup ions and atmospheric atoms (see, e.g., Lipatov and Combi, 2006; Lipatov et al., 2012).

The neutral atmosphere of Titan serves as a source of new ions, mainly by electron impact ionization from the magnetosphere plasma and also by photoionization. The neutral atmosphere also serves as collisional targets for charge exchange with the magnetospheric  $\text{H}^+$  and  $\text{O}^+$  ions. The impacting ions consist of both upstream torus ions and newly implanted ions which are picked up by the motional electric field.

We have adopted a three-species description for the neutral exosphere of the Chamberlain’s form

$$n_{\text{neutral},k} = n_{\text{atmos},k} \exp(-(1/r - 1/r_{\text{exobase}}) h_{\text{atmos},k}) \quad (13)$$

This represents a numerical approximation of the exosphere model for Titan (see, e.g., Amsif et al., 1997 and Sittler et al., 2009, 2010). In Eq. (13),  $n_{\text{atmos},k}$  is the maximum value of the neutral density extrapolated to the exobase, and  $r_{\text{exobase}} \approx 4000 \text{ km}$  (Yelle et al., 2006; Waite et al., 2005). Index  $k$  denotes  $\text{H}_2$ ,  $\text{CH}_4$ , and  $\text{N}_2$ . Here the spatial scales are  $h_{\text{atmos},\text{H}_2} = 2.75 \times 10^4 \text{ km}$ ,  $h_{\text{atmos},\text{CH}_4} = 8.3 \times 10^4 \text{ km}$  and  $h_{\text{atmos},\text{N}_2} = 1.77 \times 10^5 \text{ km}$ .

The production of new ions from the exosphere near Titan corresponds to

$$G_{\text{exo},k} = \nu_{i,k} n_{\text{atmos},k} \exp[(1/r - 1/r_{\text{exobase}}) h_{\text{atmos},k}]. \quad (14)$$

Here  $n_{\text{atmos},k}$  denotes the value of the neutral component density at  $r = r_{\text{exobase}}$  and  $\nu_{i,k}$  is the effective ionization rate per atom or molecule of species  $k$ , which includes the photoionization  $\nu_{\text{ph}}$ , and the electron impact ionization by the background  $\nu_{e,\text{im}}$  and the secondary  $\nu_{e^*,\text{im}}$  electrons (see Lipatov et al., 2012 for details). The thermal velocity of all newly formed pickup ions is about 0.25 km/s.



We use a model of the ionosphere that contains a shell-like immobile ionosphere at the Sun side at  $R_{\text{iono}} = 1300 \text{ km} + R_T$ :

$$n_{\text{iono}} = n_{\text{iono}, R_{\text{iono}}} \exp\left(-\frac{(r - R_{\text{iono}})^2}{\delta_{\text{iono}}^2}\right) \quad (15)$$

and simulate the ionospheric ion flux using active ion macro-particles with  $M_i = 28 \text{ amu}$ :

$$\text{flux}_{\text{iono}} = \text{flux}_{\text{iono}, R_{\text{iono}}} \exp\left(-\frac{(r - R_{\text{iono}})^2}{\delta_{\text{iono}}^2}\right), \quad (16)$$

Here  $\delta_{\text{iono}} = 200 \text{ km}$  is a characteristic spatial scale for the thickness of the ionosphere, and the total flux though ionosphere is about  $5 \times 10^{25} \text{ ion/s}$ . Initially the thermal velocity of active ion macro-particles is about  $0.25 \text{ km/s}$ . The flux (Eq. (15)) is produced by the use of a random number generator. Note that the active ionospheric ions ( $M_i = 28 \text{ amu}$ ) are used for the current computation inside the ionosphere, whereas the  $N_2^+$  ( $M_i = 28 \text{ amu}$ ) ions are generated in the exosphere. Note also that an immobile ionosphere with  $n_{\text{iono}, R_{\text{iono}}} = 6.25 \text{ ion/cm}^3$  is used in the modeling to avoid a low value of density due to fluctuations in the particle-in-cell method.

### 2.1. Initial conditions

Initially the computational domain contains only subAlfvén and subsonic background plasma flow with a homogeneous spatial distribution and a Maxwellian velocity distribution; pickup ions are not present at the initial time. The initial magnetic and electric fields are  $\mathbf{B} = \mathbf{B}_0$  and  $\mathbf{E} = -\mathbf{U}_0 \times \mathbf{B}_0/c$  respectively. Inside Titan the initial electromagnetic fields are  $\mathbf{E} = 0$  and  $\mathbf{B} = \mathbf{B}_0$ , and the bulk velocities of ions and electrons are also equal to zero.

### 2.2. Boundary conditions

At  $t > 0$  we begin to inject the pickup ions with a distribution according to Eq. (14). Far upstream ( $x = -13L$ , where  $L = R_T$ ), the ion flux is assumed to have a Maxwellian distribution

$$f = n_{\infty} (\pi v_{th}^2)^{-3/2} \exp\left[-\frac{(\mathbf{v} - \mathbf{U})^2}{2v_{th}^2}\right], \quad (17)$$

where  $v_{th}$  and  $\mathbf{U}$  are the thermal and the bulk velocities of the background plasma flow respectively.

At the downstream boundary we use a “Sommerfeld” radiation condition for the magnetic field, and a free escape condition for particles, with re-entry of a portion of the particles from the outflow plasma. Note that a “Sommerfeld” condition allows the waves to leave the computational domain through the back boundary (see, e.g., Tikhonov and Samarskii, 1963).

Inside Titan, the electromagnetic fields are  $\mathbf{E} = 0$  and  $\mathbf{B} = \mathbf{B}_0$ , and the bulk velocities of ions and electrons are also equal to zero.

We also take into account the effect of the finite conductivity of Titan's body so that

$$\sigma_{\text{eff}} = \sigma_{\text{up}} \quad \text{for } r > R_T + H_{\text{atmos}},$$

$$\sigma_{\text{eff}} = \sigma_{\text{iono}} \quad \text{for } R_T < r \leq R_T + H_{\text{atmos}},$$

$$\sigma_{\text{eff}} = \sigma_T \quad \text{for } r \leq R_T.$$

We have chosen the effective magnetic Reynolds number ( $R_m = 4\pi U_0 L \sigma_{\text{eff}} / c^2$ ) in the same way as was done for the T9 flyby in Lipatov et al. (2012). The effective magnetic Reynolds numbers of the upstream and ionospheric plasmas are  $R_{m, \text{up}} = 200$  and  $R_{m, \text{iono}} = 2\text{--}200$  respectively, whereas for Titan's body the magnetic Reynolds number is  $R_{m, T} = 0.2\text{--}2$ . The electromagnetic field may penetrate through Titan's interior due to the weak conductivity assumed in the Titan model.

On the flank boundaries ( $y = \pm DY/2$  and  $z = \pm DZ/2$ ), periodic boundary conditions were imposed for incoming flow particles and the electromagnetic field. The pickup ions exit the computational domain when they intersect the surfaces  $y = \pm (DY/2 - 5 \times \Delta y)$ , or  $z = \pm (DZ/2 - 5 \times \Delta z)$ , or  $x = 14L - 5 \times \Delta x$ . Thus there is no influx of pickup ions at the flank boundaries. At Titan's surface,  $r = R_T$ , the particles are absorbed. There is no boundary condition for the electromagnetic field, and we also use our equations for the electromagnetic field, Eqs. (4)–(5) and (10) inside Titan but with internal conductivity and a bulk velocity that is calculated from the particles. In this way the jump in the electric field is due to the variation of the value of the conductivity and bulk velocity across Titan's surface. Note that the position of Titan is  $x = 0, y = 0, z = 0$ .

Our code solves Eqs. (1)–(17). We used algorithm with an implicit time integration for the electric field. Note again that our code drops the first and the third collisional terms on the right-hand side of Eq. (3). The code also drops the third and fifth terms on the right-hand side of Eq. (10). The charge exchange was performed in the same manner as was done for the T9 flyby in Lipatov et al. (2012).

The three-dimensional computational domain has dimensions  $DX = 27L$ ,  $DY = 30L$ , and  $DZ = 30L$ , where  $L = R_T = 2575 \text{ km}$ . We used meshes of  $271 \times 301 \times 301$  grid points. The total number of macro-particles was  $4.5 \times 10^8$  (protons and  $O^+$ ),  $6 \times 10^7$  ( $H_2^+$ ),  $3 \times 10^7$  ( $CH_4^+$ ),  $1.5 \times 10^7$  ( $N_2^+$ ), and  $2 \times 10^6$  (active ionospheric ions) for a homogeneous mesh computation. Thus, we have about 16 macro-particles (protons and oxygen ions) per cell in the upstream region at the beginning of the modeling. We also have about 1 macro-particle (pickup ions) per cell at the external boundary of the halo and about 1600 macro-particles per cell near the exobase. The time step for particle pushing ( $\Delta t_p = 0.16 \text{ s}$ ) satisfies the condition  $U_0 \Delta t \leq \min(\Delta x, \Delta y, \Delta z)/8$ , whereas the time step for the electromagnetic equation is  $\Delta t_{EB} = 0.005 \text{ s}$ .

The global physics in Titan's environment is controlled by a set of dimensionless independent parameters such as  $M_A$ ,  $\beta_i$ ,  $\beta_e$ ,  $M_{pi}/M_p$ , ion production and charge exchange rates, diffusion lengths, and the ion gyroradius  $\epsilon = \rho_{ci}/R_T$ . Here  $\rho_{ci} = U_0/(eB/M_i c)$  and the ion plasma frequency  $\omega_{pi} = \sqrt{4\pi n_0 e^2/M_i}$ . For real values of the magnetic field, gyroradii are about 200–400 km ( $H_2^+$  background ion), 1600–3200 km ( $O^+$  background ion), 200–400 km ( $H_2^+$  pickup ion), and 1500–3000 km ( $CH_4^+$  pickup ion), which are calculated from the local bulk velocity. The grid spacing has the value  $\Delta x = 257.5 \text{ km}$ .

In order to study ion kinetic effects (e.g., excitation of low-frequency oscillations ( $\omega \ll \Omega_b$ ) by the mass loading), we must satisfy the condition  $\Delta x \leq (10\text{--}20)c/\omega_{pb}$ , where  $\Omega_b$  and  $\omega_{pb}$  denote the gyrofrequency and the plasma frequency for background ions (Winske et al., 1985) respectively. The above estimation of the plasma parameters shows that we have good resolution for the low-frequency waves. To excite high-frequency waves ( $\Omega_b \ll \omega \ll \Omega_e$ ) we must satisfy the condition  $\Delta x \leq 0.25c/\omega_{pb}$  (Winske et al., 1985) for background ions. The above estimation shows that we have insufficient resolution for the high-frequency waves.

## 3. Results of the modeling

During the TA flyby of Titan by the Cassini spacecraft, the observational data from the Cassini Plasma Spectrometer (CAPS) (Young et al., 2004) and Cassini magnetometer (MAG) (Dougherty et al., 2004) show significant variability in the surrounding plasma environments as a function of time and location. At closest approach (CA), which occurred at 1530 UT (see Fig. 1), the subsolar location was at  $70^\circ\text{E}$ ,  $23^\circ\text{S}$  in the reference frame indicated earlier, and Titan was located at 10.6 h Saturn local time (LT). CAPS data

show that the inbound electron number density varied from  $0.07 \text{ cm}^{-3}$  to  $1.92 \text{ cm}^{-3}$  between 1300 UT and 1500 UT, giving an average value of about  $0.41 \text{ cm}^{-3}$ .

The electron temperature values ranged between 6.6 eV and 97.2 eV giving a mean value around 32.7 eV (corresponding to  $3.8 \times 10^5 \text{ K}$ ). CAPS data also show a significant difference between the inbound and outbound values in the electron density. The average outbound (from 1600 UT to 1800 UT) electron density decreased significantly to  $0.23 \text{ cm}^{-3}$ . The electron temperature varied from 13.2 eV to 98.7 eV, with the averaged electron temperature slightly larger than the inbound value. The CAPS ion data indicated an upstream speed between 120 and 160 km/s according to Szego et al. (2005). The magnetic field data from MAG team show that the averaged inbound magnetic field is very different from the mean outbound magnetic field.

Thus, it is difficult to define a set of appropriate values for the upstream plasma parameters to set up the modeling. Both the magnetic field and the electron density are chosen as the averages of the inbound and outbound values, as it was done in Ma et al. (2006). The  $\text{O}^+/\text{H}^+ = 2$  ion density ratio for upstream was taken to be that observed during the Voyager 1 (Neubauer, 1992; Neubauer et al., 1984). This ratio is also in a good agreement with plasma parameters observed by the Cassini Plasma Spectrometer instrument over the first 4.5 years of its mission in orbit around Saturn (Thomsen et al., 2010). Finally, the following sets of the magnetospheric plasma and ionosphere parameters were adopted in accordance with flyby observational data: upstream velocity (from Voyager 1 data),  $U_0 = 120 \text{ km/s}$  in  $x$ ,  $y$ , and  $z$  directions,  $\mathbf{U}_0 = (111.0, -21.0, 41.0) \text{ km/s}$ ; densities (from Voyager 1 data),  $n_{\text{H}^+} = 0.1 \text{ cm}^{-3}$ ;  $n_{\text{O}^+} = 0.2 \text{ cm}^{-3}$ ; magnetic field (from MAG data),  $B_0 = 6.0 \text{ nT}$ ;  $\mathbf{B}_0 = (1.25, 3.0, -5.0) \text{ nT}$ ; Alfvén speed,  $V_A = 72 \text{ km/s}$ ; ion and electron betas (from Voyager 1 data):  $\beta_{\text{H}^+} = 0.27$  ( $T_{\text{H}^+} = 210 \text{ eV}$ );  $\beta_{\text{O}^+} = 8.07$  ( $T_{\text{O}^+} = 2.9 \text{ keV}$ );  $\beta_{e,0} = 0.83$ ;

( $T_e = 200 \text{ eV}$ );  $\beta_{e,\text{pickup}} = 0.025\text{--}0.25$ ; ( $T_{e,\text{pickup}} = 5\text{--}50 \text{ eV}$ );  $\beta_{e,\text{iono}} = 0.006$  ( $T_e = 1 \text{ eV}$ ). Total upstream beta is  $\beta = 9.17$ . Alfvén and sonic Mach numbers are  $M_A = 1.76$  and  $M_S = 0.59$  respectively. The neutral densities at the exobase were chosen from observations during the first Cassini flyby (Yelle et al., 2006):  $n_{\text{atmos},\text{H}_2} = 8.0 \times 10^5 \text{ cm}^{-3}$ ,  $n_{\text{atmos},\text{CH}_4} = 1.2 \times 10^6 \text{ cm}^{-3}$ ,  $n_{\text{atmos},\text{N}_2} = 1.2 \times 10^7 \text{ cm}^{-3}$ . The initial total production rates due to photoionization and electron impact ionization are  $Q_{\text{H}_2^+} = 1.34 \times 10^{24} \text{ ion/s}$ ;  $Q_{\text{CH}_4^+} = 3.2 \times 10^{24} \text{ ion/s}$ ;  $Q_{\text{N}_2^+} = 4.5 \times 10^{25} \text{ ion/s}$ .

In this section we discuss the results of a modeling at time  $t = 8T_{\text{transit}}$ , where  $T_{\text{transit}}$  denotes a transit time for the flow based on bulk velocity from the left (upstream) boundary to the right (downstream) boundary.

### 3.1. Global structure of Titan's environment (TA encounter)

The global interaction between magnetospheric plasma and Titan's atmosphere for the TA encounter differs from the global interaction for the T9 encounter due to different positions of Titan inside Saturn's magnetosphere and orientation of the corotation velocity relative to the Sun and magnetic field. The absence of  $\text{O}^+$  magnetospheric ions during the T9 encounter also changes the physics of the plasma environment near Titan. The T9 trajectory provides good conditions for studying the plasma processes inside the plasma wake, whereas the TA trajectory allows us also to study the composition and dynamics of the electrons, neutral and ionized components inside the ionosphere.

Fig. 2 (top) shows the asymmetrical coma-like distribution of  $\text{H}_2^+$  pickup ions for the TA encounter. A three-tail higher density distribution of the  $\text{H}_2^+$  pickup ions is merged in the coma distribution. The  $\text{H}_2^+$  pickup ions are created by photoionization and electron impact ionization in our model. The figures also

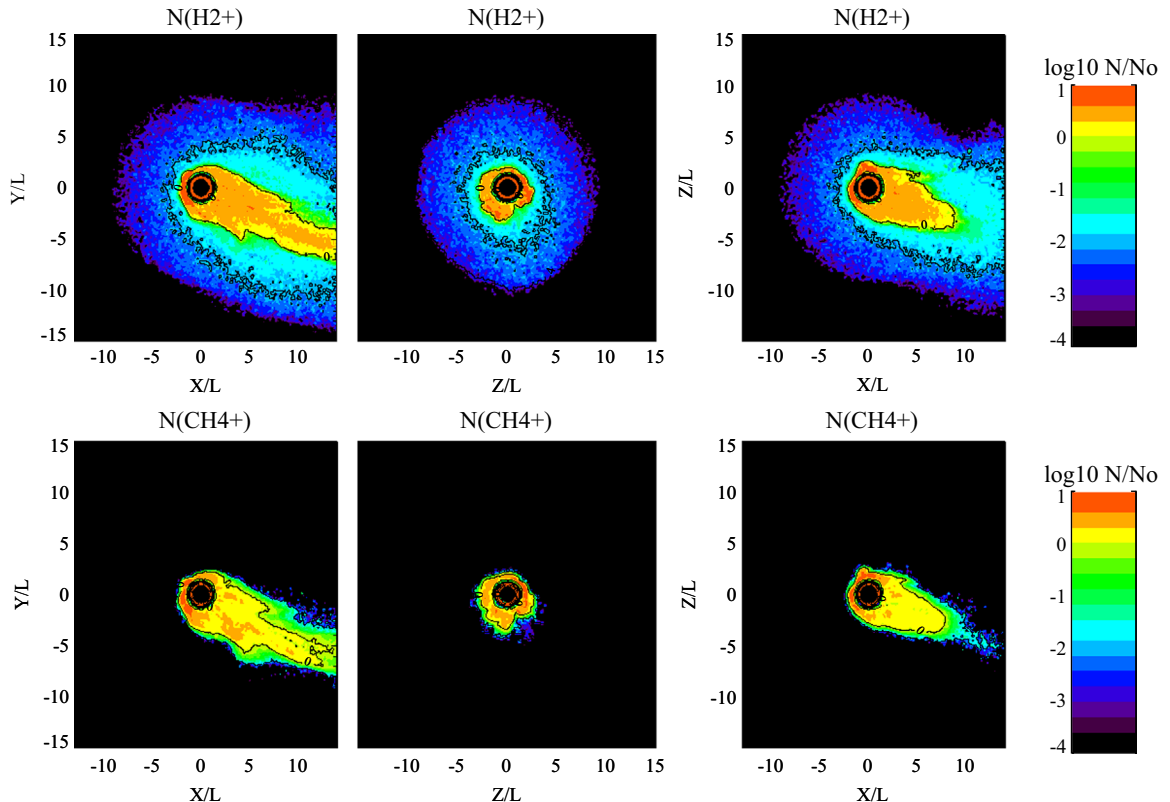


**Fig. 2.** 2-D cuts of the pickup ( $\text{H}_2^+$ ,  $\text{CH}_4^+$ ) ion density profiles. Here  $x$ - $y$  cuts (left column) are located at  $z=0$ ,  $y$ - $z$  cuts (middle column) are located at  $x=0$ ,  $x$ - $z$  cuts (right column) are located at  $y=0$  and  $N_0 = 0.3 \text{ cm}^{-3}$ .

demonstrate the formation of a sharp boundary which separates the pickup  $\text{H}_2^+$  ion low-density external region and high-density tail structure. Fig. 2 (left, top) also shows the splitting of the  $\text{H}_2^+$  pickup ion plasma wake along the magnetic field for high production rate  $\text{CH}_4^+$  and  $\text{N}_2^+$  pickup ions.

The asymmetry of the light pickup ion density profile correlates with the asymmetry of the heavy pickup ion densities due to finite gyroradius effects of the heavy pickup ion dynamics (Fig. 2, bottom). Fig. 2 (bottom) shows a  $\text{CH}_4^+$  pickup ion density distribution.  $\text{CH}_4^+$  pickup ions create a wide plasma wake, Fig. 2 (bottom). The formation of the split structure of the plasma wake (main tail and two additional weak tails) may be explained by a large gyroradius and polarization electric field caused by the gradient of the electron pressure in Eq. (10). Near the exobase, the parallel electric field is mainly determined by the electron pressure and it is oriented out of exosphere. Such finite gyroradius effects (time-dependent structuring and splitting of the pickup ion tails) were also observed in 2.5 D hybrid and bi-fluid modeling of a weak comet (see, e.g., Lipatov et al., 1997; Sauer et al., 1996, 1997; Lipatov, 2002).

The model demonstrates two spatial scales in the physics of the interaction between the background plasma and the pickup ions due to the difference in the gyroradius of the light  $\text{H}^+$  ( $\rho_{ci,\text{H}^+} = 200\text{--}400$  km) and heavy  $\text{O}^+$  ( $\rho_{ci,\text{O}^+} = 1600\text{--}3200$  km) background species (see Fig. 3, top and bottom). The heavy background  $\text{O}^+$  ions penetrate deeper inside the exosphere because of the larger gyroradius (Fig. 3, bottom). Inside the plasma wake, the density of the background ions becomes low.

The model also demonstrates an asymmetrical front in the density distribution of the background  $\text{H}^+$  ions in the  $x$ – $y$  plane (Fig. 3, top). In the region with  $y > 0$ , the front transition has a diffuse structure, whereas in the region with  $y < 0$  the front transition has a jump-like structure. The asymmetrical distribution

of the incoming ions in the  $y$ – $x$  plane may be explained by the existence of the  $B_z$  component of the upstream magnetic field (Fig. 4). The angle between the plasma tail and the upstream bulk velocity (Fig. 3) is due to pickup ion gyromotion and it depends strongly on the total pickup ion production as it was observed in case of weak comets (see, e.g., Lipatov et al., 1997).

The results of the measurements by the particles and field instruments on the Cassini spacecraft during the TA encounter provided new and important information with which realistic simulations for the plasma interaction can be tested. Along that trajectory (TA) physical signatures of the wake were seen by the Langmuir Probe (LP) as one strong peak with an electron density ( $n_e \approx 10^3 \text{ cm}^{-3}$ ) near the closest approach (CA) ( $t = 1530$  UT) when the spacecraft was inside the ionosphere, and in the electron spectrometer (CAPS-ELS) as two weaker peaks ( $t = 1454$  UT and  $t = 1600$  UT) in the electron density (see, e.g., Coates, 2009).

Fig. 5 shows the electron density along the Cassini trajectory from the ELS-CAPS measurements (red bullets) from Coates (2009) and the electron density from the RPWS LP data (red solid line) from Wahlund et al. (2005) during the TA flyby. The densities of the pickup ions and upstream ions produced in the 3D hybrid simulations are also shown: the total pickup ion density –  $N_{pi,tot}$  (solid line), the light pickup ion density –  $\text{H}_2^+$  (\*), the heavy pickup ion densities –  $\text{N}_2^+$  density ( $\diamond$ ) and  $\text{CH}_4^+$  ( $\times$ ), the active ionospheric ion density –  $M = 28$  amu ( $\circ$ ), and the background ion densities –  $\text{H}^+$  ( $\square$ ) and  $\text{O}^+$  ( $+$ ). Here, Time (h) denotes the universal time at different positions of the spacecraft along the trajectory (TA).

The model produces a total pickup ion density profile that has a maximum value very close to the peak in the electron density observed with the Langmuir Probe in Wahlund et al. (2005) (red solid line) at time  $t = 1530$  UT, Fig. 5. The main input in the peak value near  $t = 1530$  UT is due to ionospheric ( $M_i = 28$ ) and pickup ( $\text{CH}_4^+$ ,  $\text{N}_2^+$ )

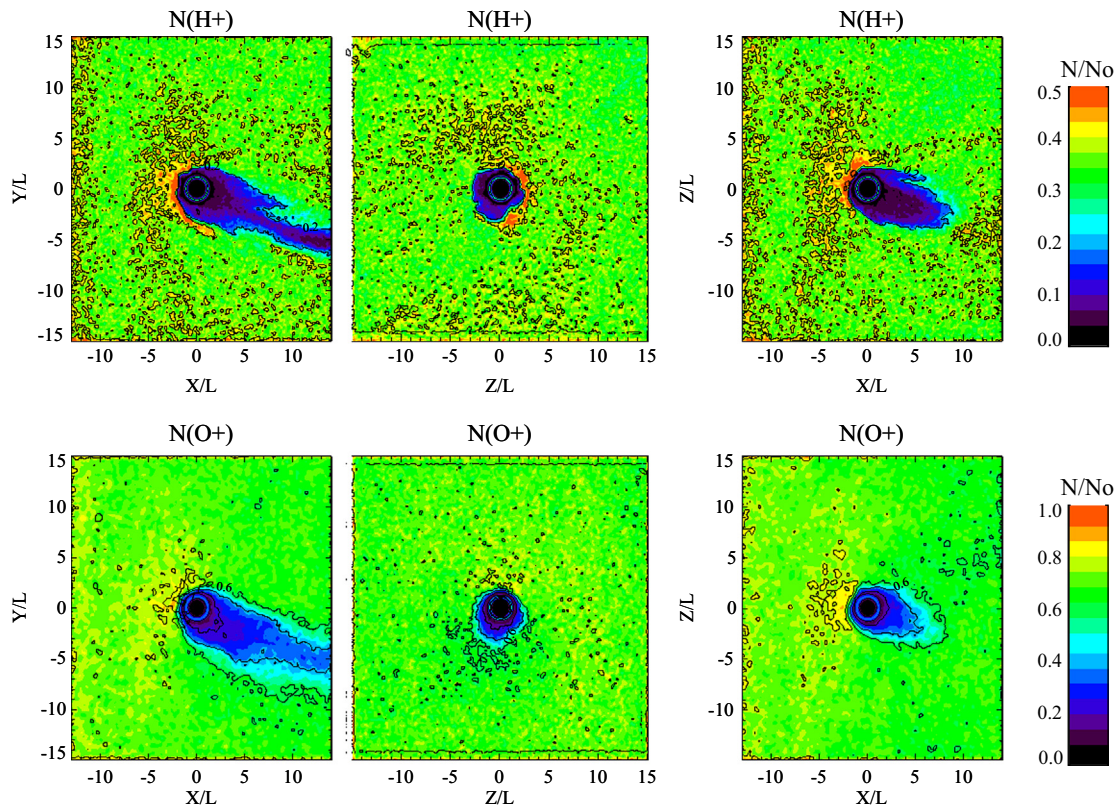
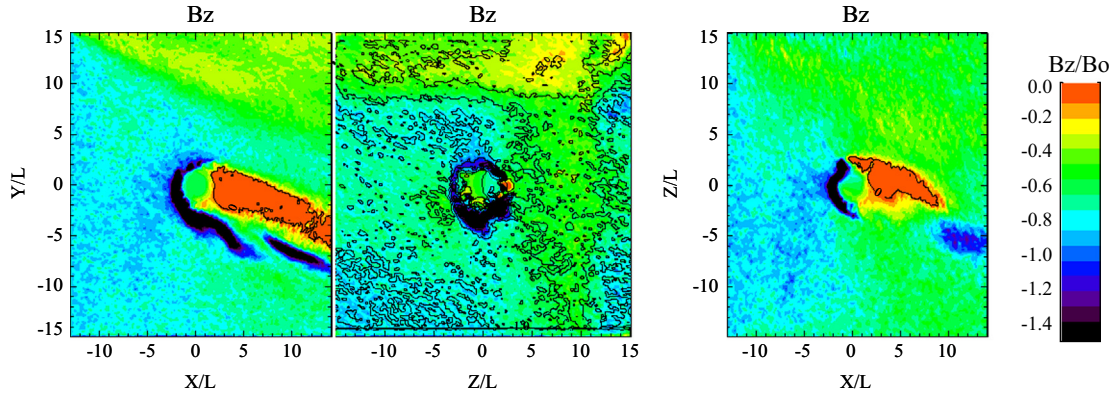
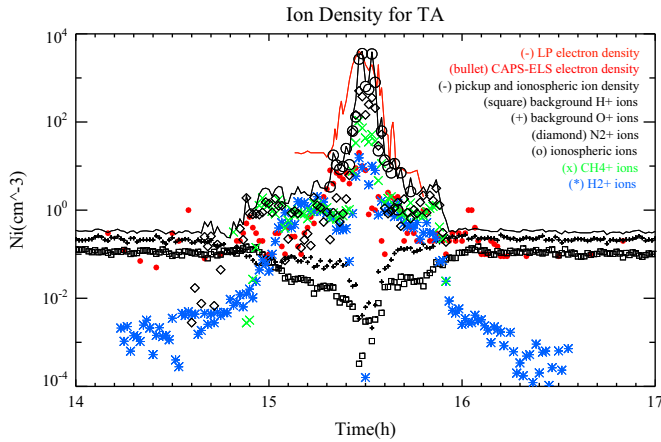


Fig. 3. 2-D cuts of the background ( $\text{H}^+$ ,  $\text{O}^+$ ) ion density profiles. Here  $x$ – $y$  cuts (left column) are located at  $z/L = 0$ ,  $y$ – $z$  cuts (middle column) are located at  $x = 0$ ,  $x$ – $z$  cuts (right column) are located at  $y = 0$  and  $N_0 = 0.3 \text{ cm}^{-3}$ .





**Fig. 4.** 2-D cuts of the magnetic field component  $B_z$ . Here  $x$ - $y$  cuts (left column) are located at  $z/L=0$ ,  $y$ - $z$  cuts (middle column) are located at  $x=0$ ,  $x$ - $z$  cuts (right column) are located at  $y=0$  and  $B_0=6.0$  nT.



**Fig. 5.** Ion densities  $N_i$  along the Cassini trajectory. The observation densities are red solid line (RPWS-LP) and red bullets (CAPS-ELS). The model densities are black, green and blue symbols. The time in the  $x$ -axis is relative to universal time UT. (For interpretation of the references to color in this figure caption, the reader is referred to the web version of this paper.)

ions. Two peaks in the total ion density at time  $t=1450$ – $1518$  UT and at time  $t=1542$ – $1556$  UT may be explained by the formation of sharp interface between regions with high and low pickup ion ( $\text{CH}_4^+$ ,  $\text{N}_2^+$ ) densities. The total ion density produced in the hybrid modeling of Modolo and Chanteur (2008) and in the MHD modeling of Ma et al. (2006) also show a good agreement with the RPWS LP observations of the electron density. At the inbound draping boundary, the simulated total ion density is about  $0.3 \text{ cm}^{-3}$  from Modolo and Chanteur (2008) and  $2 \text{ cm}^{-3}$  from Ma et al. (2006). At the outbound draping boundary, the simulated total ion density is about  $3 \text{ cm}^{-3}$  from Modolo and Chanteur (2008) and  $0.3 \text{ cm}^{-3}$  from Ma et al. (2006). Both hybrid and MHD models of Titan's plasma environment (TA flyby) could be further improved, when the ion fluid parameters derived from velocity moments of the CAPS IMS data will appear in the literature.

### 3.2. Velocity distribution function (VDF) of the background and pickup ions

Let us consider now the background and pickup ion VDF dynamics inside Titan's plasma environment obtained from a model simulation. We have computed the VDF over a spatial cube with sides  $3\Delta x \times 3\Delta y \times 3\Delta z$  in order to smooth the VDF. Fig. 6 demonstrates the evolution of the VDF for  $\text{H}^+$ ,  $\text{O}^+$  background and  $\text{H}_2^+$  pickup ions along the trajectory of the TA encounter for the following time points: (a)  $t=1430$  UT and (b)  $t=1500$  UT.

The model shows the dynamics of the Maxwellian-like VDF of the  $\text{H}^+$  and  $\text{O}^+$  background ions due to mass loading (Fig. 6, top and middle rows). At positions along the inbound part of the trajectory (Sect. (a)) the value of the transverse temperature (across the magnetic field) is comparable or larger than the value of the parallel temperature (along the magnetic field). We assume that the temperature anisotropies are connected with compression/decompression of the magnetic field.

The pickup ion dynamics are very complicated due to the inhomogeneous distribution of the source of these ions. Also, the mass loading of Saturn's magnetospheric flow by heavy ions results in a strong deceleration of the bulk velocity and the motional electric field. The electromagnetic turbulence may also result in the formation of a VDF with a Maxwellian-like core and a shell-like halo in the downstream flow.

In the outer region of the exosphere, the VDFs of the  $\text{H}_2^+$  pickup ions are ring-like distributions for  $t=1430$  UT (Fig. 6, left, bottom). The modeling shows a strong transformation in the VDF of  $\text{H}_2^+$  pickup ions from a ring-like distribution to a Maxwellian-like core and a shell-like halo. One may observe a diffusion of the particles from the thin ring distribution ( $t=1430$  UT) to a thicker ( $t=1500$  UT) ring distribution with a Maxwellian core along the trajectory. The spatial relaxation scale for that diffusion is about 25,000 km for the  $\text{H}_2^+$  pickup ions. The Maxwellian VDF is connected with creation and pickup acceleration of  $\text{H}_2^+$  ions at the region with stronger mass loading and, hence, with a more reduced bulk velocity of the background  $\text{H}^+$  ions.

In the outer region of the exosphere, the VDF of the  $\text{CH}_4^+$  pickup ions had been expected to be ring-like distributions. However, we observe VDFs which include a weak halo and Maxwellian-like core due to the following two circumstances. First,  $\text{CH}_4^+$  pickup ions begin their motion in the region with a small bulk velocity due to mass loading of the background plasma with  $\text{H}_2^+$  pickup ions. Second, the  $\text{CH}_4^+$  pickup ion production source has a smaller spatial scale than that of  $\text{H}_2^+$  pickup ions. To observe ring-like VDFs for  $\text{CH}_4^+$  and  $\text{N}_2^+$  pickup ions we have to create heavy pickup ions (macro-particles) in the outer region of the exosphere with much smaller weight function but this results in a significant increase of computational resources. To reduce the numerical "shot" noise we use variable mass macro-particles for generation of the heavy pickup ions initial spatial distribution (see, e.g., Lipatov, 2012).

The ring-type of the VDF for  $\text{H}_2^+$  pickup ions observed in modeling could cause the generation of ion cyclotron waves; however, the background thermalized light ion components will efficiently damp the waves (Cowee et al., 2010). The heavy pickup ions  $\text{CH}_4^+$  and  $\text{N}_2^+$  from the outer exosphere could also generate ion cyclotron waves, but their gyroperiods are larger than the convection time though the exosphere of Titan (Cowee et al.,



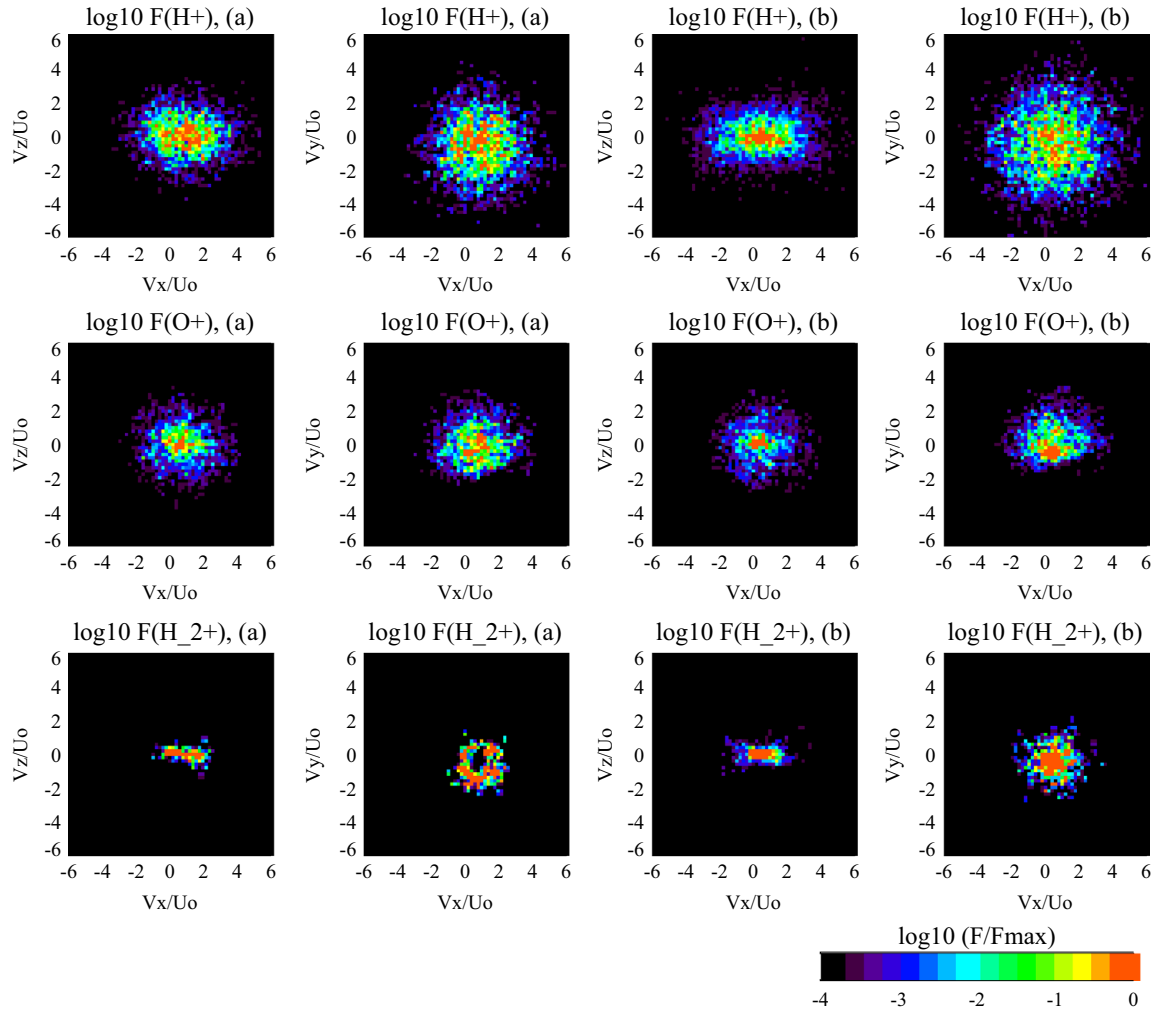


**Fig. 6.** Background  $H^+$  (top),  $O^+$  (middle), and pickup  $H_2^+$  (bottom) ion VDF along the Cassini TA trajectory. (a) Located at time  $t = 1430$  UT and (b) located at time  $t = 1500$  UT and  $U_0 = 120$  km/s.

2010). In this report, the heavy pickup ions have an isotropic-like VDF and, hence, cannot generate the ion cyclotron waves. Future modeling with variable mass macro-particles will produce a ring VDF for heavy pickup ions and may demonstrate the generation of these waves in the distant plasma wake.

Fig. 7 demonstrates the comparison between the model and observed magnetic field along the Cassini TA trajectory (Dougherty et al., 2004; Backes et al., 2005). Distribution of the  $B_x$ ,  $B_y$  and  $B_z$  components is in good agreement with observations in the region outside of the ionosphere, Fig. 7 (top, middle and bottom). Inside the ionosphere, observations show strong fluctuations in  $B_x$  and  $B_z$  components which are not reproduced in the hybrid simulation. MHD simulation of the TA case produces fluctuations in the magnetic field inside the ionosphere, probably due to a much more complicated multicomponent ionospheric model including the chemistry (Ma et al., 2006). However, the MHD model of Ma et al. (2006) does not include the Hall term in the general Ohm's law. For typical parameters of the TA flyby this term becomes very important due to the large gyroradius of the background  $O^+$  ions and the high Alfvén Mach number ( $M_A = 1.76$ ).

#### 4. Conclusions

The hybrid (true ion kinetic) model of Titan's environment produces the correct (ring/shell combined with Maxwellian) ion velocity distribution functions dynamics. On the contrary, the

multi-fluid/MHD models operate with Maxwellian ion velocity distributions that result in incorrect description of the wave-particle interactions. Our modeling demonstrated several new features of the Saturn's magnetosphere–Titan interaction during the TA encounter:

- For the TA encounter, the pickup ions create a three-tail structure: the main tail and two weak additional tails. Our model produces a satisfactory agreement in the total ion density with RPWS LP observations inside the ionosphere near closest approach and with CAPS-ELS near the inbound and outbound boundaries. The main peak at  $t = 15.30$  h was produced by ionospheric ( $M = 28m_p$ ) and pickup ( $CH_4^+$ ,  $N_2^+$ ) ions. The second and third peaks in the total density were produced in our model by jumps in the  $H_2^+$ ,  $CH_4^+$ ,  $N_2^+$  pickup ion density profile.
- The essential part of our modeling is the presence of  $O^+$  heavy ions in the background plasma in accordance with the CAPS measurements. TA encounter modeling produces a different picture of the plasma–Titan interaction from that of T9 encounter because of deeper penetration of the heavy background ions into the ionosphere. The MHD and Hall-MHD models, which also include the heavy ions in the background plasma, produce only one wide peak in the density profile (Ma et al., 2006).
- The model shows a dynamics of the Maxwellian-like VDF of the  $H^+$ ,  $O^+$  background ions due to mass loading.
- The model also shows a strong transformation in the VDF of the  $H_2^+$  and  $CH_4^+$  pickup ions near the sharp external boundary of

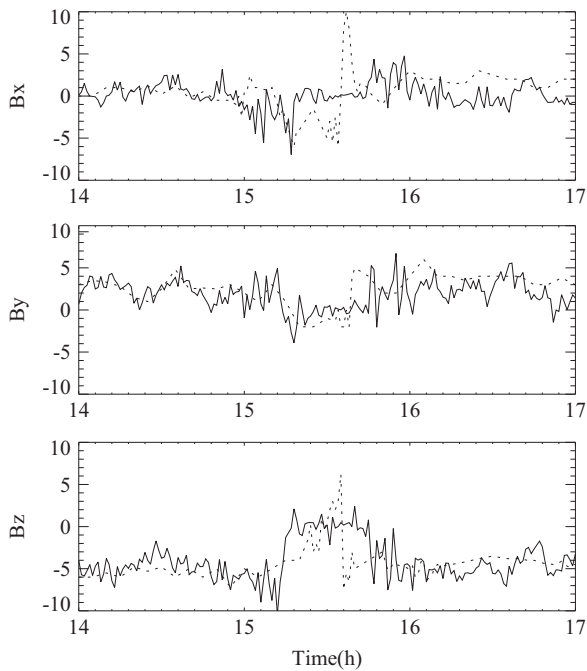


**Fig. 7.** Variations in the magnetic field along the Cassini TA trajectory. Solid line – computation, dashed line – observation. The time in the x-axis is relative to universal time UT.

exosphere. (From a quasi-ring distribution to a quasi-Maxwellian core and shell-like halo.)

- The non-Maxwellian velocity distribution may serve as a key factor in the interaction between ions and the neutral component in Titan's environment.
- The magnetic field in the model is in agreement with observations along the Cassini TA trajectory except near closest approach. The strong oscillations in the magnetic field observed near closest approach are probably due to the current generated inside the ionosphere. A better agreement between observations and modeling requires further improvement in the ionosphere model and not the other way around.
- Future modeling must use the composite grid structure, e.g., “Cubed sphere” grid (see, e.g., Koldoba et al., 2002 and references therein) to resolve the multiscale effects near the surface of Titan and in the outer plasma environment.

## Acknowledgments

A.S.L., E.C.S., R.E.H., J.F.C., and D.G.S. were supported by the Grant *Analysis of Titan's Interaction with Saturn's Magnetosphere using Cassini Titan Flyby Data and Kinetic-Fluid Model* from the NASA Cassini Data Analysis Program (08-CDAP08-0043, PI – E.C. Sittler Jr.). A.S.L. was also supported in part by the grants/tasks 900-37-172 and 670-90-315 between the GPHI UMBC and NASA GSFC. Computational resources (supercomputers Endeavour and Pleiades (Ivy Bridge)) were provided by the NASA Ames Advanced Supercomputing (NAS) Division (Projects SMD-09-1124 and SMD-13-1517). The authors thank the referees for fruitful comments.

## References

- Amsif, A., Dandouras, J., Roelof, E.C., 1997. Modeling the production and imaging of energetic neutral atoms from Titan's exosphere. *J. Geophys. Res.* 102 (A10), 22169–22181.
- Backes, H., et al., 2005. Titan's magnetic field signature during the first Cassini encounter. *Science* 308, 992.
- Braginskii, S.L., 1965. Transport processes in a plasma. In: Leontovich, M.A. (Ed.), *Reviews of Plasma Physics*. Consultants Bureau, New York, pp. 205–240.
- Brecht, S.H., Luhmann, J.G., Larson, D.J., 2000. Simulation of the Saturnian magnetospheric interaction with Titan. *J. Geophys. Res.* 105 (A6), 13119–13130.
- Coates, A.J., 2009. Interaction of Titan's ionosphere with Saturn's magnetosphere. *Philos. Trans. R. Soc. A* 367, 773–788, <http://dx.doi.org/10.1098/rsta.2008.0248>.
- Cowee, M.M., Gary, S.P., Wei, H.Y., Tokar, R.L., Russell, C.T., 2010. An explanation for the lack of ion cyclotron wave generation by pickup ions at Titan: 1-D hybrid simulation results. *J. Geophys. Res.* 115, A10224, <http://dx.doi.org/10.1029/2010JA015769>.
- Cravens, T.E., Lindgren, C.J., Ledvina, S.A., 1998. A two-dimensional multifluid MHD model of Titan's plasma environment. *Planet. Space Sci.* 46 (9/10), 1193–1205.
- Dougherty, M.K., et al., 2004. The Cassini magnetic field investigation. *Space Sci. Rev.* 114, 331.
- Hartle, R.E., Sittler, E.C., Ogilvie, K.W., Scudder, J.D., Lazarus, A.J., Atreya, S.K., 1982. Titan's ion exosphere observed from Voyager 1. *J. Geophys. Res.* 87, 1383–1394.
- Hartle, R.E., Sittler, E.C., Neubauer, F., et al., 2006. Initial interpretation of Titan plasma interaction as observed by the Cassini plasma spectrometer: comparisons with Voyager 1. *Planet. Space Sci.* 54, 1211–1224.
- Kabin, K., Gombosi, T., De Zeeuw, D., Powell, K., Israelevich, P., 1999. Interaction of the Saturnian magnetosphere with Titan: results of a three-dimensional MHD simulation. *J. Geophys. Res.* 104 (A2), <http://dx.doi.org/10.1029/1998JA900080.6536>.
- Kabin, K., Israelevich, P., Ershkovich, A., Neubauer, F., Gombosi, T., De Zeeuw, D., Powell, K., 2000. Interaction of the Saturnian magnetosphere with Titan: results of a three-dimensional MHD simulation. *J. Geophys. Res.* 104 (A2), <http://dx.doi.org/10.1029/1998JA900080.6536>.
- Kallio, E., Sillanpää, I., Janhunen, P., 2004. Titan in subsonic and supersonic flow. *Geophys. Res. Lett.* 31, L15703, <http://dx.doi.org/10.1029/2004GL020344>.
- Kallio, E., Sillanpää, I., Jarvinen, R., Janhunen, P., Dougherty, M., Bertucci, C., Neubauer, F., 2007. Morphology of the magnetic field near Titan: hybrid model study of the Cassini T9 flyby. *Geophys. Res. Lett.* 34, L24S09, <http://dx.doi.org/10.1029/2007GL030827>.
- Keller, C.N., Cravens, T.E., 1994. One-dimensional multispecies hydrodynamic models of the wakeside ionosphere of Titan. *J. Geophys. Res.* 99 (A4), 6527–6536.
- Koldoba, A.V., Romanova, M.M., Ustyugova, G.V., Lovelace, R.V.E., 2002. Three dimensional MHD simulation of accretion to an inclined rotator: the “cubed sphere” method. *Astrophys. J.* 576, L53–L56.
- Ledvina, S.A., Cravens, T.E., 1998. A three-dimensional MHD model of plasma flow around Titan. *Planet. Space Sci.* 46 (9/10), 1175–1191.
- Ledvina, S.A., Cravens, T.E., Kecskeméty, K., 2005. Ion distributions in Saturn's magnetosphere near Titan. *J. Geophys. Res.* 110, A06211, <http://dx.doi.org/10.1029/2004JA010771>.
- Ledvina, S.A., Brecht, S.H., 2012. Consequences of negative ions for Titan's plasma interaction. *Geophys. Res. Lett.* 39, L20103.
- Ledvina, S.A., Brecht, S.H., Cravens, T.E., 2012. The orientation of Titan's dayside ionosphere and its effects on Titan's plasma interaction. *Earth Planets Space* 64, 207–230.
- Lipatov, A.S., 2002. The Hybrid Multiscale Simulation Technology: An Introduction with Application to Astrophysical and Laboratory Plasmas. Springer-Verlag, Berlin, Heidelberg, New York.
- Lipatov, A.S., 2012. Merging for particle-mesh complex particle kinetic modeling of the multiple plasma beams. *J. Comput. Phys.* 231, 3101–3118.
- Lipatov, A.S., Combi, M.R., 2006. Effects of kinetic processes in shaping Io's global plasma environment: a 3D hybrid model. *ICARUS* 180 (2), 412–427.
- Lipatov, A.S., Motschmann, U., Bagdonat, T., 2002. 3-D hybrid simulation of the interaction of the solar wind with a weak comet. *Planet. Space Sci.* 50, 403–411.
- Lipatov, A.S., Sauer, K., Baumgärtel, K., 1997. 2.5-D hybrid code simulation of the solar wind interaction with weak comets and related objects. *Adv. Space Res.* 20 (2), 279.
- Lipatov, A.S., Sittler Jr., E.C., Hartle, R.E., 2007a. Titan's plasma environment for TA encounters: 3D hybrid simulation and comparison with observations. In: *Proceeding of Spring AGU Meeting, Acapulco, Mexico*, May 16–22.
- Lipatov, A.S., Sittler Jr., E.C., Hartle, R.E., 2007b. 3D hybrid simulation of the Titan's plasma environment. Session M6. In: *Proceeding of European Planetary Science Congress 2007*, Potsdam, Germany, 20–24 August.
- Lipatov, A.S., Sittler Jr., E.C., Hartle, R.E., 2007c. 3D hybrid simulation of the Titan's plasma environment, Division of Plasma Physics 2007 Meeting of the American Physical Society, ID: DPP07-2007-000034, 12–16 November, 2007, Orlando, FL.
- Lipatov, E.C., Sittler Jr., E.C., Hartle, R.E., Cooper, J.F., Simpson, D.G., 2011. Background and pickup ion velocity distribution dynamics in Titan's plasma environment: 3D hybrid simulation and comparison with CAPS T9 observations. *Adv. Space Res.* 48, 1114–1125.
- Lipatov, A.S., Sittler, E.C., Hartle, R.E., Cooper, J.F., Simpson, D.G., 2012. Saturn's magnetosphere interaction with Titan for T9 encounter: 3D hybrid simulation and comparison with CAPS's observations. *Planet. Space Sci.* 61, 66–78.
- Lipatov, A.S., Zank, G.P., Pauls, H.L., 1998. The interaction of neutral interstellar H with the heliosphere: a 2.5-D particle-mesh Boltzmann simulation. *J. Geophys. Res.* 103 (A12), 29679.
- Mankofsky, A., Sudan, R.N., Denavit, J., 1987. Hybrid simulation of ion beams in background plasma. *J. Comput. Phys.* 70, 89–116.
- Ma, Y.-J., Nagy, A.F., Cravens, T.E., Sokolov, I.V., Hansen, K.C., Wahlund, J.-E., Cray, F.J., Coates, A.J., Dougherty, M.K., 2006. Comparisons between MHD model calculations and observations of Cassini flybys of Titan. *J. Geophys. Res.* 111, A05207, <http://dx.doi.org/10.1029/2005JA011481>.

- Ma, Y.-J., Nagy, A.F., Toth, G., Cravens, T.E., Russell, C.T., Gombosi, T.I., Wahlund, J.-E., Crary, F.J., Coates, A.J., Bertucci, C.L., Neubauer, F.M., 2007. 3D global multi-species Hall-MHD simulation of the Cassini T9 flyby. *Geophys. Res. Lett.* 34, L24S10, <http://dx.doi.org/10.1029/2007GRL031627>.
- Modolo, R., Chanteur, G.M., Wahlund, J.-E., Canu, P., Kurth, W.S., Gurnett, D., Matthews, A.P., Bertucci, C., 2007a. Plasma environment in the wake of Titan from hybrid simulation: a case study. *Geophys. Res. Lett.* 34, L24S07, <http://dx.doi.org/10.1029/2007GL030489>.
- Modolo, R., Wahlund, J.-E., Boström, R., Canu, P., Kurth, W.S., Gurnett, D., Lewis, G.R., Coates, A.J., 2007b. Far plasma wake of Titan from RPWS observations: a case study. *Geophys. Res. Lett.* 34, L24S04, <http://dx.doi.org/10.1029/2007GL030482>.
- Modolo, R., Chanteur, G.M., 2008. A global hybrid model for Titan's interaction with the Kronian plasma: application to the Cassini Ta flyby. *J. Geophys. Res.* 113, A01310, <http://dx.doi.org/10.1029/2007JA012453>.
- Nagy, A.F., Liu, Y., Hansen, K.C., Kabin, K., Gombosi, T.I., Combi, M.R., DeZeeuw, D.L., Powell, K.G., Kliore, A.J., 2001. The interaction between the magnetosphere of Saturn and Titan's ionosphere. *J. Geophys. Res.* 106, 6151–6160.
- Ness, N.F., Acuna, M.H., Behannon, K.W., 1982. The induced magnetosphere of Titan. *J. Geophys. Res.* 87, 1369–1381.
- Neubauer, F.M., 1992. Titan's magnetospheric interaction. In: Kaldeich, B. (Ed.), *Symposium on Titan*. European Space Agency Special Publications, ESA SP-338, pp. 267–272.
- Neubauer, F., Gurnett, D.A., Scudder, J.D., Hartle, R.E., 1984. Titan's magnetospheric interaction. In: Gehrels, T., Matthews, M.S. (Eds.), *Saturn*. University of Arizona Press, Tucson, pp. 760–787.
- Sauer, K., Bogdanov, A., Baumgärtel, K., Dubinin, E., 1996. Plasma environment of comet Wirtanen during its low-activity stage. *Planet. Space Sci.* 44 (7), 715–729.
- Sauer, K., Lipatov, A.S., Baumgärtel, K., Dubinin, E., 1997. Solar wind-pluto interaction revised. *Adv. Space Res.* 20 (2), 295.
- Sillanpää, I., Kallio, E., Janhunen, P., Schmidt, W., Mursula, K., Vilpola, J., Tanskanen, P., 2006. Hybrid simulation study of ion escape at Titan for different orbital positions. *Adv. Space Res.* 28, 799–805.
- Simon, S., Kleindienst, G., Boesswetter, A., Bagdonat, T., Motschmann, U., Glassmeier, K.-H., Schule, J., Bertucci, C., Dougherty, M., 2007. Hybrid simulation of Titan's magnetic field signature during the Cassini T9 flyby. *Geophys. Res. Lett.* 34, L24S08, <http://dx.doi.org/10.1029/2007GLO29967>.
- Sittler Jr, E.C., Hartle, R.E., Vinäs, A.F., Johnson, R.E., Smith, H.T., Mueller-Wodarg, I., 2005. Titan interaction with Saturn's magnetosphere: Voyager 1 results revisited. *J. Geophys. Res.* 110, A09302, <http://dx.doi.org/10.1029/2004JA010759> 1253.
- Sittler, E.C., Hartle, R.E., Bertucci, C., Coates, A., Cravens, T., Dandouras, I., Shemansky, D., 2009. Energy deposition processes in Titan's upper atmosphere and its induced magnetosphere. In: Brown, R.H., Lebreton, J.P., Waite, J.H. (Eds.), *Titan from Cassini–Huygens*. Springer, Dordrecht, Heidelberg, London, New York, pp. 393–455.
- Sittler, E.C., Hartle, R.E., Johnson, R.E., Cooper, J.F., Lipatov, A.S., Bertucci, C., Coates, A.J., Szego, K., Shappirio, M., Simpson, D.G., Wahlund, J.-E., 2010. Saturn's magnetospheric interaction with Titan as defined by Cassini encounters T9 and T18: new results. *Planet. Space Sci.* 58, 327–350.
- Snowden, D., Winglee, R., Bertucci, C., Dougherty, M., 2007. Three-dimensional multifluid simulation of the plasma interaction at Titan. *J. Geophys. Res.* 112, A12221, <http://dx.doi.org/10.1029/2007JA012393>.
- Szego, K., et al., 2005. The global plasma environment of Titan as observed by Cassini plasma spectrometer during the first two close encounters with Titan. *Geophys. Res. Lett.* 32, L20S05, <http://dx.doi.org/10.1029/2005GL022646>.
- Tikhonov, A.N., Samarskii, A.A., 1963. *Equations of Mathematical Physics*. Macmillan, New York p. 765.
- Thomsen, M.F., Reisenfeld, D.B., Delapp, D.M., Tokar, R.L., Young, D.T., Crary, F.J., Sittler, E.C., McGraw, M.A., Williams, J.D., 2010. Survey of ion plasma parameters in Saturn's magnetosphere. *J. Geophys. Res.* 115, A10220, <http://dx.doi.org/10.1029/2010JA015267>.
- Wahlund, J.-E., Boström, R., Gustafsson, G., Gurnett, D.A., Kurth, W.S., Pederson, A., Averkamp, T.F., Hospodarsky, G.B., Persoon, A.M., Canu, P., Neubauer, F.M., Dougherty, M.K., Eriksson, A.I., Moroka, M.W., Gill, R., Andre, M., Eliasson, L., Müller-Wodarg, I., 2005. Cassini measurements of cold plasma in the ionosphere of Titan. *Science* 308 (5724), 986–989.
- Waite, J.H., et al., 2005. Ion neutral mass spectrometer results from the first flyby of Titan. *Science* 308, 986–989, <http://dx.doi.org/10.1126/science.1110652>.
- Winske, D., Wu, C.S., Li, Y.Y., Mou, Z.Z., Guo, S.Y., 1985. Coupling of newborn ions to the solar wind by electromagnetic instabilities and their interaction with the bow shock. *J. Geophys. Res.* 90, 2713–2726.
- Yelle, R.V., Borggren, N., de la Haye, V., Kasprzak, W.T., Niemann, H.B., Müller-Wodarg, I., Waite Jr, J.H., 2006. The vertical structure of Titan's upper atmosphere from Cassini Ion neutral mass spectrometer measurements. *Icarus* 182, 567–576.
- Young, D., et al., 2004. Composition and dynamics of plasma in Saturn's magnetosphere. *Science* 307, 1262–1266.